

Role of Heme Types in Heme-Copper Oxidases: Effects of Replacing a Heme *b* with a Heme *o* Mimic in an Engineered Heme-Copper Center in Myoglobin[§]

Ningyan Wang,[†] Xuan Zhao,[‡] and Yi Lu^{*,†,‡}

Contribution from the Department of Biochemistry, and Department of Chemistry, University of Illinois at Urbana-Champaign, Urbana, Illinois 61801

Received April 25, 2005; E-mail: yi-lu@uiuc.edu

Abstract: To address the role of the secondary hydroxyl group of heme *a/o* in heme-copper oxidases, we incorporated Fe(III)-2,4 (4,2) hydroxyethyl vinyl deuterioporphyrin IX, as a heme *o* mimic, into the engineered heme-copper center in myoglobin (sperm whale myoglobin L29H/F43H, called Cu_BMb). The only difference between the heme *b* of myoglobin and the heme *o* mimic is the substitution of one of the vinyl side chains of the former with a hydroxyethyl group of the latter. This substitution resulted in an ~4 nm blue shift in the Soret band and ~20 mV decrease in the heme reduction potential. In a control experiment, the heme *b* in Cu_BMb was also replaced with a mesoheme, which resulted in an ~13 nm blue shift and ~30 mV decrease in the heme reduction potential. Kinetic studies of the heme *o* mimic-substituted Cu_BMb showed significantly different reactivity toward copper-dependent oxygen reduction from that of the *b*-type Cu_BMb. In reaction with O₂, Cu_BMb with a native heme *b* showed heme oxygenase activity by generating verdoheme in the presence of Cu(I). This heme degradation reaction was slowed by ~19-fold in the heme *o* mimic-substituted Cu_BMb (from 0.028 s⁻¹ to 0.0015 s⁻¹), while the mesoheme-substituted Cu_BMb shared a similar heme degradation rate with that of Cu_BMb (0.023 s⁻¹). No correlation was found between the heme reduction potential and its O₂ reactivity. These results strongly suggest the critical role of the hydroxyl group of heme *o* in modulating heme-copper oxidase activity through participation in an extra hydrogen-bonding network.

Heme-copper oxidases (HCOs) are a superfamily of terminal oxidases of the electron-transfer chain in both eukaryotic mitochondria and bacteria.^{1–4} They catalyze oxygen reduction to water and convert the liberated free energy into a proton gradient across the membrane. This proton gradient can then be used by ATP synthases to synthesize ATP, a universal energy source for many cellular processes. All HCOs contain a low-spin bis-His coordinated heme as an electron-transfer center, and a high-spin heme-copper center where oxygen binding, activation, and reduction occurs (Figure 1A).^{5–10} The high-spin

[†] Department of Biochemistry, University of Illinois at Urbana-Champaign.

[‡] Department of Chemistry, University of Illinois at Urbana-Champaign.

[§] Abbreviations: HCO, heme-copper oxidase; CcO, cytochrome *c* oxidase; Mb, myoglobin; Cu_BMb(*b*), F43H/L29H sperm whale Mb; Cu_BMb(*o*), Cu_BMb incorporated with the heme *o* mimic; Cu_BMb(*m*), Cu_BMb incorporated with mesoheme; HVD, 2,4 (4,2)-monohydroxyethyl vinyl deuterioporphyrin IX; HO, heme oxygenase.

- (1) Babcock, G. T.; Wikström, M. *Nature* **1992**, *356*, 301–309.
- (2) Garcia-Horsman, J. A.; Barquera, B.; Rumbley, J.; Ma, J.; Gennis, R. B. *J. Bacteriol.* **1994**, *176*, 5587–5600.
- (3) Ferguson-Miller, S.; Babcock, G. T. *Chem. Rev.* **1996**, *96*, 2889–2907.
- (4) Namslauer, A.; Brzezinski, P. *FEBS Lett.* **2004**, *567*, 103–110.
- (5) Tsukihara, T.; Aoyama, H.; Yamashita, E.; Tomizaki, T.; Yamaguchi, H.; Shinzawa-Itoh, K.; Nakashima, R.; Yaono, R.; Yoshikawa, S. *Science* **1995**, *269*, 1069–1074.
- (6) Yoshikawa, S.; et al. *Science* **1998**, *280*, 1723–1729.
- (7) Tsukihara, T.; Aoyama, H.; Yamashita, E.; Tomizaki, T.; Yamaguchi, H.; Shinzawa-Itoh, K.; Nakashima, R.; Yaono, R.; Yoshikawa, S. *Science* **1996**, *272*, 1136–1144.
- (8) Iwata, S.; Ostermeier, C.; Ludwig, B.; Michel, H. *Nature* **1995**, *376*, 660–669.
- (9) Ostermeier, C.; Harrenga, A.; Ermiler, U.; Michel, H. *Proc. Natl. Acad. Sci. U.S.A.* **1997**, *94*, 10547–10553.

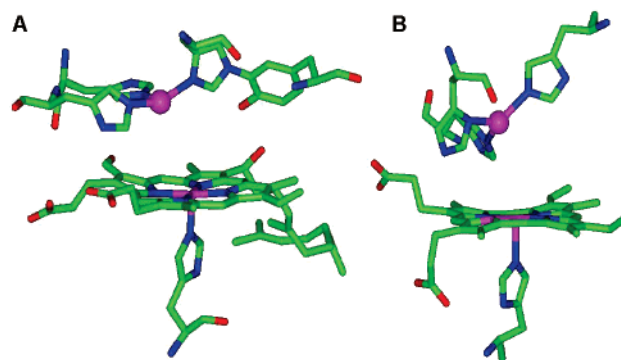


Figure 1. (A) Crystal structure of the heme-copper center of bovine heart CcO (ref 6). (B) The active site of a computer model of Cu_BMb(*b*).

heme in the heme-copper center was found to be mostly *a*- or *o*-type heme in eukaryotic and most bacterial HCOs.^{11,12} However, *b*-type heme has been recently discovered in a new subfamily of cytochrome oxidases called cytochrome *ccb*₃ from proteobacteria.¹³

- (10) Abramson, J.; Riistama, S.; Larsson, G.; Jasaitis, A.; Svensson-Ek, M.; Laakkonen, L.; Puustinen, A.; Iwata, S.; Wikstrom, M. *Nat. Struct. Biol.* **2000**, *7*, 910–917.
- (11) Puustinen, A.; Finel, M.; Virkki, M.; Wikstrom, M. *FEBS Lett.* **1989**, *249*, 163–167.
- (12) Puustinen, A.; Wikstrom, M. *Proc. Natl. Acad. Sci. U.S.A.* **1991**, *88*, 6122–6126.
- (13) Pitcher, R. S.; Watmough, N. *J. Biochim. Biophys. Acta* **2004**, *1655*, 388–399.

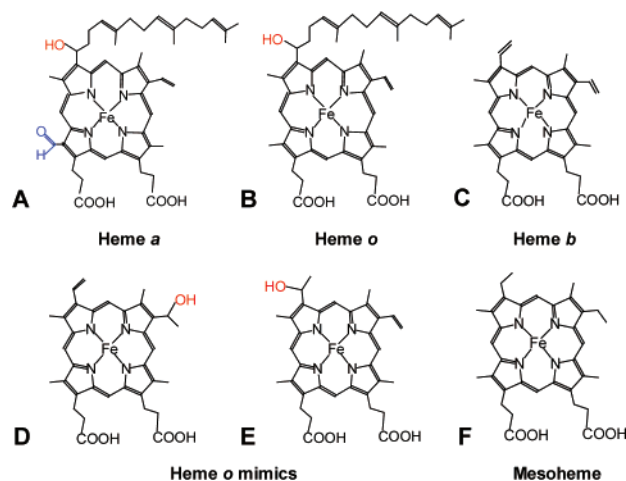


Figure 2. Heme types found in the heme-copper center of HCOs and the structure of the *o*-type heme mimic: (A) heme *a*; (B) heme *o*; (C) heme *b*; (D and E) isomers of heme *o* mimic used in our protein model study; (F) mesoheme.

Heme *a* and *o* are derivatives of protoheme IX (heme *b*) in which the vinyl group on pyrrole ring A is substituted by a 17-carbon hydroxyethylfarnesyl group (Figure 2). In addition, heme *a* contains a formyl group on pyrrole ring D in place of the methyl group in heme *o* and *b*. The HCOs containing *a*- and *o*-type high-spin hemes are highly related in structure and function, while the HCOs containing *b*-type high-spin heme are different from other HCOs, not only in the heme prosthetic group, but also in functional properties such as oxygen binding affinity.¹⁰ Furthermore, the *b*-type HCOs have no sequential or structural homology with the more common *a/o*-type HCOs.^{13,14}

Because of the above structural differences between heme types, it is natural to ask the question how much these differences contribute to the functional properties of HCOs. To answer this question, it is desirable to replace one type of heme with another type in the same protein environment. The role of the heme type in the electron-transfer function of the low-spin heme has been addressed earlier in both native and de novo designed protein model systems.^{15,16} However, the role of heme type in the high-spin heme-copper center has been studied only through heme promiscuity, where different types of hemes were found to be in the heme-copper center of the bacterial HCOs purified from mutant strains or cells grown under different conditions. It was shown that HCOs remained mostly active when heme substitution occurred between *a*- and *o*-type hemes, despite possible switching between the quinol and cytochrome *c* oxidase activity.^{17–21} However, when either *a*- or *o*-type heme was replaced by heme *b* at the high-spin site, the enzyme lost its activity.^{22,23} These observations suggested the importance

of the hydroxyethylfarnesyl side chain of heme *a/o* for proper enzyme function. Defects in the maturation of the hydroxyethylfarnesyl heme side chain were also recognized as important causes of diseases in yeast and human.²⁴ As for the biological function of the side chain, its highly hydrophobic farnesyl group was generally considered to anchor the heme at the correct position in the enzyme. On the other hand, the hydroxyl group of the farnesyl side chain is located at the end of the K-channel and is close enough to be hydrogen-bonded to the hydroxyl group of the tyrosine that is covalently attached to one of the histidine ligands to Cu_B.²⁵ In proposed HCO mechanisms, the farnesyl hydroxyl has been suggested to be an essential part of the active site hydrogen-bonding network, with internal water molecules bridging the gap between the tyrosine hydroxyl group and the bound oxygen at the heme-copper site.^{26,27}

While studying HCOs with a different type of heme at the high-spin heme-copper center has offered a number of clues to the role of heme types in HCOs, it has been difficult to separate the effect of the long hydrophobic chain of the farnesyl group from that of the hydroxyl group. In addition, spectroscopic signatures of the heme-copper center in HCOs are almost always dominated by that of the low-spin heme center, and they can be deduced only from difference spectra when the low-spin spectra are subtracted, making it difficult to characterize the important intermediate forms of the center. Although small molecule synthetic models of HCOs can help focus on the heme-copper center without interference from the low-spin heme, it has been difficult to synthesize models with a similar structure while containing different heme types because the hemes are often modified to position functional groups for binding the copper center or to increase solubility in an organic solvent.^{28,29} Therefore, it is desirable to prepare a model heme-copper protein where the heme can be exchanged with other types, such that the only difference is the hydroxyl group.

Previously, we reported the design and engineering of a heme-copper center into sperm whale myoglobin by computer modeling and site-directed mutagenesis (since it contains a native heme *b*, it will be called Cu_BMb(*b*) in this paper).³⁰ The model protein contains three histidines capable of coordinating to a novel copper center at the distal site of the heme (Figure 1B). Since myoglobin is small, easy to produce, and free of other interfering chromophores, spectroscopic studies of the model protein have provided new insights into the role of Cu_B, protons and small ligands such as chloride in modulating functional properties of the heme-copper center such as reduction potentials and O₂ binding and reduction.^{31–34} One nice

(14) de Gier, J.-W. L.; et al. *J. Mol. Microbiol.* **1996**, *20*, 1247–1260.

(15) Puustinen, A.; Morgan, J. E.; Verkhovskii, M.; Thomas, J. W.; Gennis, R. B.; Wikstrom, M. *Biochemistry* **1992**, *31*, 10363–10369.

(16) Gibney, B. R.; Isogai, Y.; Rabanal, F.; Reddy, K. S.; Grosset, A. M.; Moser, C. C.; Dutton, P. L. *Biochemistry* **2000**, *39*, 11041–11049.

(17) Contreras-Zentella, M.; Mendoza, G.; Membrillo-Hernandez, J.; Escamilla, J. E. *J. Biol. Chem.* **2003**, *278*, 31473–31478.

(18) Schroter, T.; Winterstein, C.; Ludwig, B.; Richter, O.-M. H. *FEBS Lett.* **1998**, *432*, 109–112.

(19) Sone, N.; Fujiwara, Y. *FEBS Lett.* **1991**, *288*, 154–158.

(20) Peschek, G. A.; Alge, D.; Fromwald, S.; Mayer, B. *J. Biol. Chem.* **1995**, *270*, 27937–27941.

(21) Sakamoto, J.; Handa, Y.; Sone, N. *J. Biochem. (Tokyo)* **1997**, *122*, 764–771.

(22) Zickermann, I.; Tautou, O. S.; Link, T. A.; Korn, M.; Ludwig, B.; Richter, O.-M. H. *Eur. J. Biochem.* **1997**, *246*, 618–624.

(23) Hill, J.; Goswitz, V. C.; Calhoun, M.; Garcia-Horsman, J. A.; Lemieux, L.; Alben, J. O.; Gennis, R. B. *Biochemistry* **1992**, *31*, 11435–11440.

(24) Moraes, C. T.; Diaz, F.; Barrientos, A. *Biochim. Biophys. Acta* **2004**, *1659*, 153–159.

(25) Das, T. K.; Pecoraro, C.; Tomson, F. L.; Gennis, R. B.; Rousseau, D. L. *Biochemistry* **1998**, *37*, 14471–14476.

(26) Blomberg, M. R. A.; Siegbahn, P. E. M.; Wikstroem, M. *Inorg. Chem.* **2003**, *42*, 5231–5243.

(27) Kucier, R. I. *Biochim. Biophys. Acta* **2005**, *1706*, 134–146.

(28) Collman, J. P.; Boulatov, R.; Sunderland, C. J.; Fu, L. *Chem. Rev.* **2004**, *104*, 561–588.

(29) Kim, E.; Chufan, E. E.; Kamaraj, K.; Karlin, K. D. *Chem. Rev.* **2004**, *104*, 1077–1133.

(30) Sigman, J. A.; Kwok, B. C.; Lu, Y. *J. Am. Chem. Soc.* **2000**, *122*, 8192–8196.

(31) Zhao, X.; Yeung, N.; Wang, Z.; Guo, Z.; Lu, Y. *Biochemistry* **2005**, *44*, 1210–1214.

(32) Sigman, J. A.; Kim, H. K.; Zhao, X.; Carey, J. R.; Lu, Y. *Proc. Natl. Acad. Sci. U.S.A.* **2003**, *100*, 3629–3634.

(33) Zhao, X.; Nilges, M. J.; Lu, Y. *Biochemistry* **2005**, *44*, 6559–6564.

(34) Lu, Y.; Berry, S. M.; Pfister, T. D. *Chem. Rev.* **2001**, *101*, 3047–3080.

feature of this model protein is the ease of extracting and replacing its native heme *b* with another type of heme, making it possible to compare the effect of different heme types on the activity and properties of the heme-copper centers in the same protein framework.

Though a natural design would replace heme *b* with the native heme *a/o*, we choose not to introduce the long hydrophobic chain of the farnesyl group into our model system for two reasons. First, introducing native heme *a* into Mb has been shown to result in a perturbed protein attributable to the presence of the long hydrophobic chain that is not present in the native Mb.³⁵ We hypothesize that introducing a heme *o* mimic (Figure 2, parts D and E) which is very similar to heme *b* will eliminate this problem. Second, introducing the heme *o* mimic makes it possible to separate effects of the hydroxyl group and the long hydrophobic chain and allow us to address exclusively the role of the hydroxyl group in HCO reaction mechanisms. Therefore, we choose to use Fe(III)-2,4 (4,2) hydroxyethyl vinyl deuterioporphyin IX as a mimic of *o*-type heme and incorporate it into our Cu_BMb model protein. The major feature of this compound is the replacement of one vinyl group of heme *b* with a monohydroxyethyl side chain (Figure 2, parts D and E). Compared to native heme *o*, it introduces the critical secondary hydroxyl group to the heme ring without the long alkyl farnesyl chain. Here we report the synthesis and incorporation of heme *o* mimic into Cu_BMb, and demonstrate that the resulting protein (called Cu_BMb(*o*)) can serve as a close model of the heme-copper center with *o*-type heme that is free of other chromophores. In addition, we also incorporated mesoheme (Figure 2F) into Cu_BMb (called Cu_BMb(*m*)) as an hydroxyl-free artificial heme-Mb control in our studies. The study showed that Cu_BMb(*o*) demonstrated a significant difference in reactivity toward copper-dependent oxygen reduction from that of the same protein with a *b*-type heme or mesoheme.

Experimental Section

Preparation of the Heme *o* Mimic (Fe(III)-2,4 (4,2) Hydroxyethyl Vinyl Deuterioporphyin IX). 2,4 (4,2) Hydroxyethyl vinyl deuterioporphyin IX (HVD, >90%) was purchased from Frontier Scientific Inc. (Utah). The incorporation of iron into HVD was performed following literature methods^{36,37} with the following modifications: To a flask containing 5 mg of HVD and 5 mg of ferrous acetate was added 3 mL of degassed pyridine/acetic acid solution (1:50 v/v). The reaction mixture was stirred under argon in the dark at room temperature for 1 to ~1.5 h. The metallization of HVD, as indicated by the color change from red to dark brown, was monitored by UV–vis spectroscopy until no further spectral changes were observed. The resulting brown solution was then exposed to air and extracted with ice-cold ether. The ether solution was further washed with cold 12% HCl and cold water. After removal of ether under vacuum, the residue was dissolved in 2 mL of 0.1 N NaOH; after stirring on ice for 1 h, the solution was acidified with 10% HCl and the final product was extracted with ether. The removal of solvent yielded the final product with a yield of ~50%.

Preparation of Cu_BMb(*o*) and Cu_BMb(*m*). Cu_BMb(*b*) was expressed and purified from *E. coli* as described previously.³⁰ Heme *b* was extracted from the protein by Teale's method.³⁸ Immediately before

use, the heme *o* mimic or mesoheme (Frontier Scientific) was dissolved in 0.1 M NaOH. About 1 equiv of heme was titrated into the apo-protein on an ice-bath. The titration was closely monitored by UV–vis spectroscopy. The reaction mixture was stirred overnight to reach equilibrium between the heme and the protein. After centrifugation to remove aggregated components, the reaction mixtures were passed down a PD10 size exclusion column (Amersham Bioscience) to remove any excess heme.

Electronic Absorption (UV–Vis) Characterization. UV–vis spectra were obtained by using a Hewlett-Packard 8453 spectrometer equipped with water-jacketed cell holder connected to a thermostatic water bath. The samples were in 20 mM MOPS buffer at pH 8. Deoxy-Cu_BMb(*o*) was prepared by reducing met-Cu_BMb(*o*) with dithionite. Oxy-Cu_BMb(*o*) was obtained by reducing met-Cu_BMb(*o*) with excess ascorbate in air.

Kinetic Study of O₂ Reduction. The reactions of Cu_BMb(*o*) and Cu_BMb(*m*) with O₂ were studied at the same conditions as previously described for Cu_BMb(*b*).³² The met-Cu_BMb(*o*) or met-Cu_BMb(*m*) (6 μM) was mixed with 6 mM sodium ascorbate and 0.6 mM *N,N,N',N'*-tetramethyl-*p*-phenylenediamine (TMPD) in 20 mM MOPS buffer at pH 8.0. The reaction was initiated by adding 12 μM (2 equiv) CuSO₄. In addition, 340 units of bovine liver catalase were also added before the reaction as scavenger of exogenous hydrogen peroxide. The spectral changes were monitored at 410 and 657 nm for Cu_BMb(*o*) with the kinetic software (Chemstation, version A10.01) provided with the UV–vis spectrometer. The rates were calculated by fitting changes in absorbance versus time to a single-exponential equation of formation [eq 1] or decay [eq 2]. The spectral changes were monitored at 418 and 678 nm for Cu_BMb(*b*) and 404 and 610 nm for Cu_BMb(*m*). The rates of both reactions were fitted to a double-exponential equation of formation [eq 3] or decay [eq 4].

$$y = y_0 + a(1 - e^{-kt}) \quad (1)$$

$$y = y_0 + ae^{-kt} \quad (2)$$

$$y = y_0 + a(1 - e^{-k_1t}) + b(1 - e^{-k_2t}) \quad (3)$$

$$y = y_0 + ae^{-k_1t} + be^{-k_2t} \quad (4)$$

Electrospray Ionization Mass Spectrometric Analysis of Heme Degradation Products. Products of the reaction of Cu_BMb(*b*), Cu_BMb(*o*), and Cu_BMb(*m*) were analyzed by electrospray ionization spectrometry. At different time points of the reaction, identical aliquots of the reaction mixture were removed and treated with 0.5 mM EDTA and 0.5 mM KCN to terminate the reaction. The resulting solution was then passed down a size exclusion column equilibrated with ammonium acetate buffer (20 mM, pH 6.8) and concentrated for mass spectral analysis. Electrospray ionization was performed by using a Micromass (Manchester, U.K.) Quattro triple-quadrupole mass spectrometer. Mass analysis was performed in the first quadrupole (Q1), and a cone voltage of 75 V was used to induce dissociation of heme.

Electrochemistry. The reduction potentials of Cu_BMb(*o*) and Cu_BMb(*m*) were measured by a spectroelectrochemical method using an optically transparent thin layer cell (OTTLE) as previously described.^{31,39–41} The redox titration was carried out using an ~0.6 mL sample containing 0.2 mM protein, 40 μM phenazine methosulfate (Sigma), and 40 μM anthraquinone-2-sulfonate (Sigma) as mediators in 100 mM potassium phosphate buffer at pH 7.0. The sample was purged gently with argon for at least 30 min to remove O₂ before being transferred to the OTTLE cell. A model 362 potentiostat from Princeton

(35) Larsen, R. W.; Nunez, D. J.; MacLeod, J.; Shiemke, A. K.; Musser, S. M.; Nguyen Hiep, H.; Ondrias, M. R.; Chan, S. I. *J. Inorg. Biochem.* **1992**, *48*, 21–31.

(36) Marques, H. M.; Munro, O. Q.; Crawcour, M. L. *Inorg. Chim. Acta* **1992**, *196*, 221–229.

(37) Bonnett, R.; Ridge, R. J.; Scourides, P. A.; Berenbaum, M. C. *J. Chem. Soc., Perkin Trans. 1* **1981**, 3135–3140.

(38) Teale, F. W. J. *Biochim. Biophys. Acta* **1959**, *35*, 543.

(39) Taboy, C. H.; Bonaventura, C.; Crumbliss, A. L. *Methods Enzymol.* **2002**, *353*, 187–209.

(40) Hayashi, T.; Dejima, H.; Matsuo, T.; Sato, H.; Murata, D.; Hisaeda, Y. *J. Am. Chem. Soc.* **2002**, *124*, 11226–11227.

(41) Matsuo, T.; Dejima, H.; Hirota, S.; Murata, D.; Sato, H.; Ikegami, T.; Hori, H.; Hisaeda, Y.; Hayashi, T. *J. Am. Chem. Soc.* **2004**, *126*, 16007–16017.

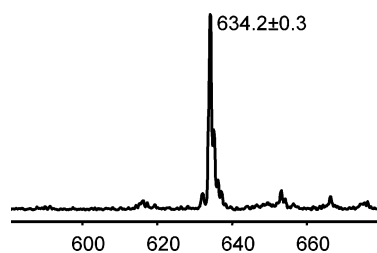


Figure 3. Electrospray mass spectrum of heme *o* mimic; calculated: 634.2.

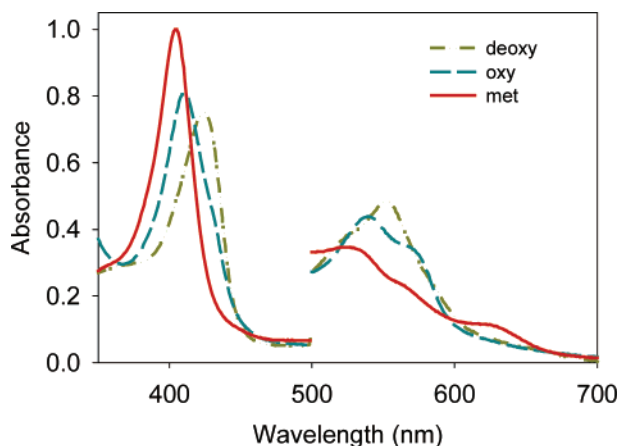


Figure 4. Optical spectra of $\text{Cu}_B\text{Mb}(o)$ in MOPS buffer (20 mM, pH 8); met- $\text{Cu}_B\text{Mb}(o)$ (red solid line); oxy- $\text{Cu}_B\text{Mb}(o)$ (blue dashed line); deoxy- $\text{Cu}_B\text{Mb}(o)$ (green dashed-dotted line).

Applied Research was used to control the potential of the working electrode. After applying the potential (typically with 25 mV increments), the UV-vis spectra were recorded using a Cary 3E spectrophotometer until no further spectral changes occurred. The Ag/AgCl (3M KCl) reference electrode was calibrated with an SCE electrode and found to be 200 mV (vs NHE). The spectroelectrochemical titration data for the entire spectra were analyzed by global analysis using singular value decomposition (SVD) and nonlinear regression modeling with SpecFit/32 (Spectrum Software Associates, Inc). The data were fit with a model of $A \leftrightarrow B$ because the Nernst plot at a single wavelength (e.g., 431 nm) is linear.

Results

Preparation of Heme *o* Mimic and $\text{Cu}_B\text{Mb}(o)$. The hydroxyl group of 2,4-(4,2)-hydroxyethyl vinyl deuterioporphyryn (HVD) is light- and heat-sensitive and can be easily converted to protoporphyrin IX under higher temperature. To avoid the dehydration of HVD, the incorporation of iron into HVD was conducted at room temperature and in the dark. The ESI-MS spectrum of the purified heme *o* mimic (Figure 3) shows a single peak (634.2 ± 0.3) corresponding to the expected value (634.2). The engineered $\text{Cu}_B\text{Mb}(b)$ was expressed in *E. coli* and purified as described previously.³⁰ After removing heme *b* from $\text{Cu}_B\text{Mb}(b)$ using the Teale's method,³⁸ the heme *o* mimic was titrated into apo- Cu_BMb until the ratio of the absorption of the heme band (404 nm) to that of the protein (280 nm) stopped increasing. The excess heme was then removed by size exclusion column.

UV-Vis Spectral Characterization. As shown in Figure 4, the UV-vis spectrum of the oxidized $\text{Cu}_B\text{Mb}(o)$ (met- $\text{Cu}_B\text{Mb}(o)$) displays a Soret band at 404 nm, and α - and β -bands at 630 and 511 nm, respectively, typical of the oxidized form of myoglobin. Compared to met- $\text{Cu}_B\text{Mb}(b)$, the Soret band of

Table 1. Spectral Properties of Wild Type Mb (wtMb), $\text{Cu}_B\text{Mb}(b)$, $\text{Cu}_B\text{Mb}(o)$, and $\text{Cu}_B\text{Mb}(m)$

	ferric			oxy			deoxy	
	Soret	vis		Soret	vis		Soret	vis
$\text{Cu}_B\text{Mb}(o)$	404	511	630	410	540	572	425	548
$\text{Cu}_B\text{Mb}(m)$	395	495	620	404	533	566	420	545
$\text{Cu}_B\text{Mb}(b)$	408	502	630	418	540	580	434	554
wtMb	409	502	632	418	542	580	434	556

Table 2. Pyridine Hemochrome Spectra of Heme *b*, Heme *o*, and Heme *o* Mimic^a

heme type	α_{max}	β_{max}
heme <i>b</i>	557	526
heme <i>o</i>	553	521
heme <i>o</i> mimic	552	520

^a Refs 12 and 43.

met- $\text{Cu}_B\text{Mb}(o)$ is blue-shifted by 4 nm (Table 1), due to the presence of a more electron-donating hydroxyethyl side chain in the heme *o* mimic. The pyridine hemochrome spectrum of the heme *o* mimic matches well with that of the native heme *o* in cytochrome *o* oxidase (Table 2).^{12,42} The reduced protein (called deoxy- $\text{Cu}_B\text{Mb}(o)$) exhibits a Soret band at 425 nm and a visible absorption band at 548 nm. When exposed to air, the deoxy- $\text{Cu}_B\text{Mb}(o)$ was converted to oxy- $\text{Cu}_B\text{Mb}(o)$, which shows absorptions at 410, 540, and 572 nm. The mesoheme-substituted $\text{Cu}_B\text{Mb}(m)$ showed absorption bands that also match to that in the literature.⁴³ For example, the Soret band of met- $\text{Cu}_B\text{Mb}(m)$ is blue-shifted to 395 nm, due to substitution of both vinyl groups with the more electron-rich ethyl groups.

Kinetic Study of O_2 Reduction. The reactions of O_2 with $\text{Cu}_B\text{Mb}(b)$, $\text{Cu}_B\text{Mb}(o)$, and $\text{Cu}_B\text{Mb}(m)$ were carried out in the presence of excess ascorbate and TMPD as described previously.³² In addition, 340 units of catalase were also added as scavenger of the exogenous peroxide to prevent its reaction with heme.⁴⁴ Addition of CuSO_4 to oxy- $\text{Cu}_B\text{Mb}(b)$ resulted in a dramatic decrease of the Soret band at 418 nm, concomitant with the appearance of visible bands at 622 and 678 nm (Figure 5A), which had been identified, respectively, as the formation of verdoheme and CO-verdoheme³² based on their spectral similarity to those of the corresponding derivatives in heme oxygenases.^{45,46} Further confirmation of verdoheme formation was based on spectral similarity of its pyridine derivative to that of verdoheme and on the molecular weight from electrospray mass spectrometry.³² The decay of the Soret band at 418 nm can be fitted to a double-exponential equation, with $k_1 = 0.028 \text{ s}^{-1}$ and $k_2 = 0.0083 \text{ s}^{-1}$. The first phase of the biphasic kinetics was assigned as heme degradation to form verdoheme (at $k_1 = 0.028 \text{ s}^{-1}$, which is identical to the rate of verdoheme formation measured at 678 nm), and the second phase was assigned as heme autoxidation (at $k_2 = 0.0083 \text{ s}^{-1}$).³²

Upon addition of CuSO_4 to oxy- $\text{Cu}_B\text{Mb}(o)$ under the same conditions, the Soret band at 410 nm also decreased over time

(42) Smith, K. M. *Porphyryns and Metalloporphyryns*, 2nd ed.; Elsevier: New York, 1975; Vol. 19, p 805.

(43) Hayashi, T.; Matsuo, T.; Hitomi, Y.; Okawa, K.; Suzuki, A.; Shiro, Y.; Iizuka, T.; Hisaeda, Y.; Ogoshi, H. *J. Inorg. Biochem.* **2002**, *91*, 94–100.

(44) Sigman, J. A.; Wang, X.; Lu, Y. *J. Am. Chem. Soc.* **2001**, *123*, 6945–6946.

(45) Wilks, A.; Ortiz de Montellano, P. R. *J. Biol. Chem.* **1993**, *268*, 22357–22362.

(46) Liu, Y.; Moeenne-Loccoz, P.; Loehr, T. M.; Ortiz de Montellano, P. R. *J. Biol. Chem.* **1997**, *272*, 6909–6917.

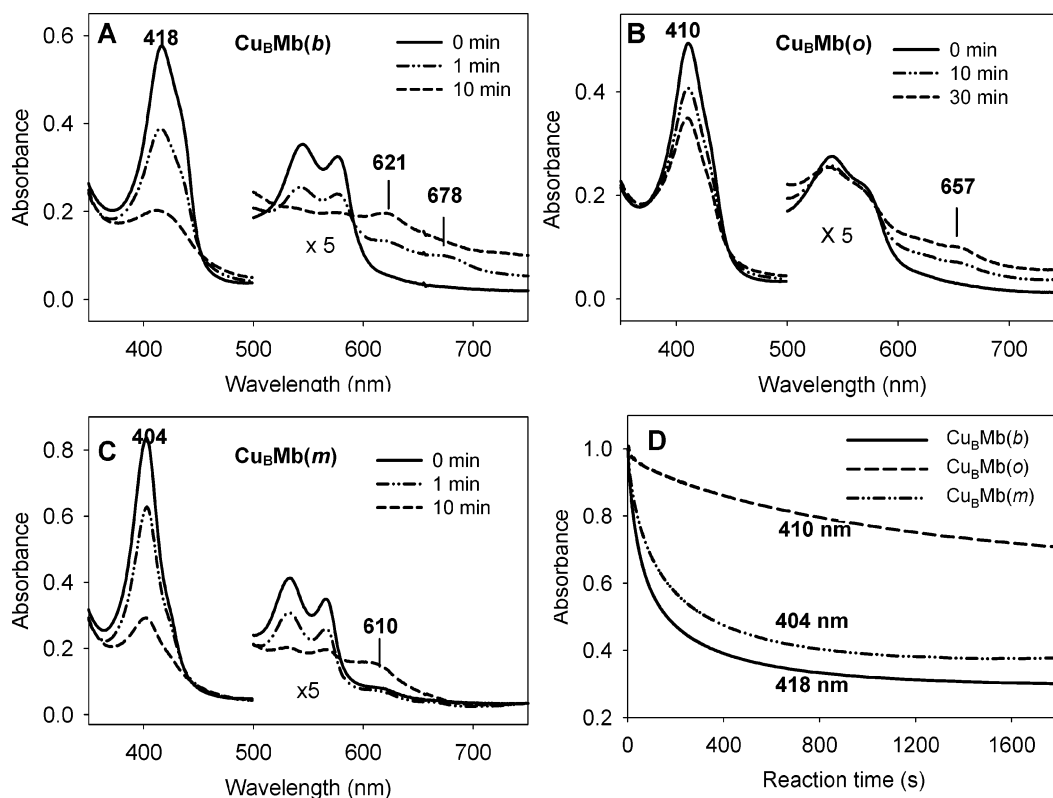


Figure 5. Reaction of $\text{Cu}_B\text{Mb}(b)$ (A), $\text{Cu}_B\text{Mb}(o)$ (B), and $\text{Cu}_B\text{Mb}(m)$ (C) with O_2 , monitored by UV-vis spectra in the presence of 1000 equiv of ascorbate, 100 equiv of TMPD, 340 units of catalase in 20 mM MOPS buffer (pH 8) at 25 °C with 2 equiv of copper. (D) The changes of Soret band absorbance were plotted against the reaction time at 418 nm for $\text{Cu}_B\text{Mb}(b)$ (solid line), at 410 nm for $\text{Cu}_B\text{Mb}(o)$ (dashed line), and at 404 nm for $\text{Cu}_B\text{Mb}(m)$ (dashed-dotted line).

and shifted toward 404 nm but with a much slower rate (Figure 5B). While nearly 50% of heme *b* in $\text{Cu}_B\text{Mb}(b)$ was converted to verdoheme within the first minute of reaction and the reaction is complete within 10 min, a substantial amount of $\text{Cu}_B\text{Mb}(o)$ still remained after 30 min of reaction and little spectral change was observed when the reaction was extended to longer time (1 h). The decay of the Soret band at 410 nm can be fitted to a single-exponential equation with a rate constant of 0.0015 s^{-1} , ~ 19 -fold slower than that of $\text{Cu}_B\text{Mb}(b)$ ($k_1 = 0.028 \text{ s}^{-1}$). As a control, the reaction of $\text{Cu}_B\text{Mb}(m)$ with O_2 under the same conditions had a rate of 0.023 s^{-1} , similar to that of $\text{Cu}_B\text{Mb}(b)$. (Figure 5C) These results indicated that the heme *o* mimic has significantly different behavior from heme *b* or mesoheme during the reduction of O_2 by Cu_BMb (Figure 5D).

The different reactivity of $\text{Cu}_B\text{Mb}(b)$, $\text{Cu}_B\text{Mb}(o)$, and $\text{Cu}_B\text{Mb}(m)$ with O_2 observed in the UV-vis spectra was also confirmed by the electrospray mass spectrometric analysis of the heme decay products (Figure 6). Upon the addition of copper, the heme *b* in $\text{Cu}_B\text{Mb}(b)$ ($m/z = 616$) was quickly converted to verdoheme ($m/z = 619$) in 9 min, with some biliverdin ($m/z = 635$) also observed (Figure 6A). The verdoheme was then further converted to biliverdin at 30 min (Figure 3). Similar results were observed for $\text{Cu}_B\text{Mb}(m)$, as most mesoheme was degraded into biliverdin ($m/z = 639$) within half an hour (Figure 6B). In contrast, the heme decay reaction in $\text{Cu}_B\text{Mb}(o)$ proceeded more slowly than that of either $\text{Cu}_B\text{Mb}(b)$ or $\text{Cu}_B\text{Mb}(m)$ (Figure 6C); after 9 min of reaction, the heme *o* mimic ($m/z = 634$) remained almost intact. Only about a quarter of heme *o* decayed into biliverdin ($m/z = 653$) after 30 min of reaction.

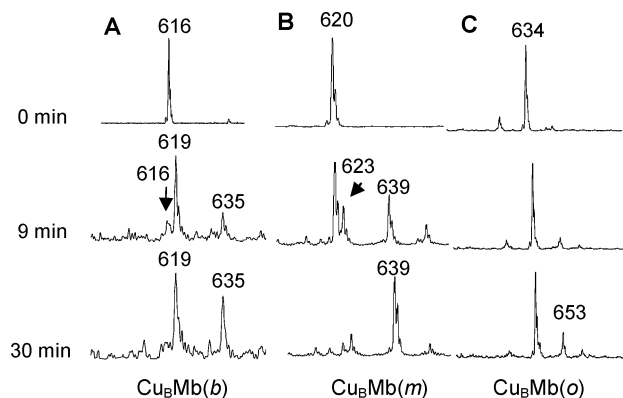


Figure 6. Electrospray ionization mass spectrometry profiles showing the reaction products of $\text{Cu}_B\text{Mb}(b)$ (A), $\text{Cu}_B\text{Mb}(m)$ (B), and $\text{Cu}_B\text{Mb}(o)$ (C) with O_2 at 0, 9, and 30 min after the reaction. Only the heme-containing region of the spectrum is shown.

In the course of heme degradation of $\text{Cu}_B\text{Mb}(b)$, verdoheme was the main product observed (Figure 6A). This result can be explained by a fast formation of CO-bound verdoheme, as observed in the UV-vis spectra, which significantly slowed its further conversion to biliverdin. In the case of heme degradation of $\text{Cu}_B\text{Mb}(o)$, biliverdin ($m/z = 653$) was observed as the main heme decay product for $\text{Cu}_B\text{Mb}(o)$ (Figure 6C). For $\text{Cu}_B\text{Mb}(m)$, verdoheme formation was observed at the early stage of reaction, but most of it was quickly converted to biliverdin (Figure 6B). These differences in reaction products may be attributable to either higher CO affinity for the *b*-type verdoheme or increased O_2 activity for the other two types of verdohemes. While the higher affinity for O_2 by verdoheme in

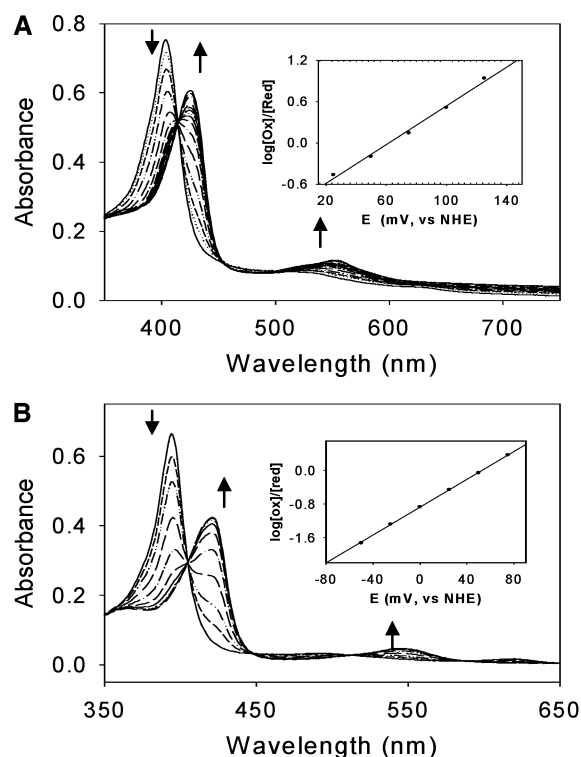


Figure 7. Spectroelectrochemical titration of $\text{Cu}_B\text{Mb}(o)$ (A) and $\text{Cu}_B\text{Mb}(m)$ (B) (100 mM potassium phosphate, pH 7, 25 °C). (Inset) Nernst plot was derived from the dependence of the absorbance at 404 nm (A) and 395 nm (B) on the applied potential.

the heme *o* mimic could be rationalized by the presence of the putative hydrogen-bonding network formed through the hydroxyl group and intervening waters, the reason for the increased O_2 affinity by the same species in mesoheme is not clear and warrants further studies.

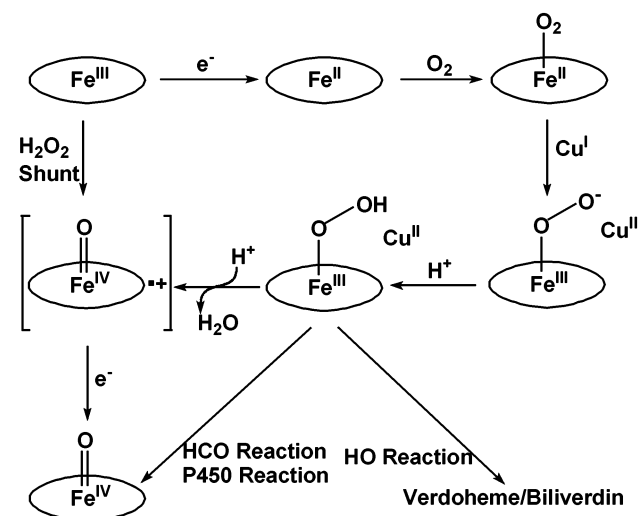
Under the identical conditions as described above, the heme degradation of $\text{Cu}_B\text{Mb}(b)$, $\text{Cu}_B\text{Mb}(o)$, or $\text{Cu}_B\text{Mb}(m)$ was not observed in the absence of copper ion or in the presence of Zn(II) or Ag(I) as redox-inactive mimics of Cu(II) and Cu(I), respectively. These control experiments strongly suggest the critical role of a redox-active copper ion in the O_2 reduction.

Redox Property of $\text{Cu}_B\text{Mb}(o)$. The effect of redox potential changes induced by incorporation of heme *o* mimic and mesoheme was investigated by spectroelectrochemical method. As shown in Figure 7, the Nernst plots of both $\text{Cu}_B\text{Mb}(o)$ and $\text{Cu}_B\text{Mb}(m)$ yielded a linear line, indicating single redox processes. The midpoint potentials of $\text{Cu}_B\text{Mb}(o)$ (Figure 7A) and $\text{Cu}_B\text{Mb}(m)$ (Figure 7B) were found to be 62 and 53 mV (vs NHE), respectively, both of which are lower than that of $\text{Cu}_B\text{Mb}(b)$ (80 mV vs NHE) under identical conditions.³¹ The decreases of reduction potential may be a result of substituting one or both electron-withdrawing vinyl side chains with more electron-donating hydroxyl ethyl group or ethyl groups that stabilizes the oxidized form of heme.

Discussion

$\text{Cu}_B\text{Mb}(o)$ May Serve as a Close Spectral Model of *o*-Type Heme-Copper Centers in HCOs. The free heme *o* mimic has a broad absorbance band at 386 nm in aqueous solution, while the optical spectra of met-, oxy- and deoxy- $\text{Cu}_B\text{Mb}(o)$ display similar well-defined absorbance spectra as those of other heme

Scheme 1 Proposed Reaction Mechanism of $\text{Cu}_B\text{Mb}(o)$ with O_2



proteins (Figure 4), suggesting that the heme *o* mimic was incorporated into the heme pocket. Due to the presence of the secondary hydroxyl group on the heme ring, free heme *o* mimic and the native heme *o* have similar features in the pyridine hemochrome spectra, both showing a 4 nm blue shift compared to that of heme *b* (Table 2). This characteristic 4 nm shift was also observed in the Soret peak of met- $\text{Cu}_B\text{Mb}(o)$ when compared to that of met- $\text{Cu}_B\text{Mb}(b)$ (Table 1). Unlike the heme *o* of the heme-copper center of HCOs, whose spectral features are always dominated by that of its low-spin heme neighbor, $\text{Cu}_B\text{Mb}(o)$ is free of other chromophores, and no difference spectrum is needed to reveal its spectral features, making it easier to study the kinetic intermediates.

$\text{Cu}_B\text{Mb}(b)$ and $\text{Cu}_B\text{Mb}(o)$ Exhibit Significantly Different Reactivity toward O_2 Reduction. Previously, we reported kinetic studies on the engineered HCO model $\text{Cu}_B\text{Mb}(b)$ with O_2 in the presence of copper ion and reductants.³² The reaction is metal dependent, as it only occurs in the presence of redox-active copper and generates verdoheme instead of oxyferryl-heme in HCO. However oxyferryl-heme was obtained when $\text{Cu}_B\text{Mb}(b)$ reacted with H_2O_2 , a species with an equivalent in oxidation state to $2e^-$ reduced O_2 , but possessing extra protons. These results indicate that proton delivery by a hydrogen-bonding network during the O_2 reaction is important to avoid heme degradation and to promote the HCO reaction (Scheme 1).³²

In the heme-copper center of HCOs, the hydroxyl group of heme *a/o* is located at the end of the K-channel for proton transportation and is also within the hydrogen-bonding distance to the histidine-cross-linked tyrosine hydroxyl group. Its position makes it a promising candidate for participation in a hydrogen-bonding network involving water that could be responsible for aiding O_2 reduction at the heme-copper center.^{26,27} The importance of proton delivery by hydrogen-bonding networks has also been proposed to be responsible for the different reactivity of heme oxygenase and cytochrome P450, another heme enzyme that shares a similar ferryl intermediate to that of HCOs.^{47,48} We hypothesize that introduction of the hydroxyl group through

(47) Fujii, H.; Zhang, X.; Tomita, T.; Ikeda-Saito, M.; Yoshida, T. *J. Am. Chem. Soc.* **2001**, *123*, 6475–6484.

(48) Matsui, T.; Furukawa, M.; Unno, M.; Tomita, T.; Ikeda-Saito, M. *J. Biol. Chem.* **2005**, *280*, 2981–2989.

the heme *o* mimic into the Cu_BMb active site may restore some of the proton delivery network through hydrogen bonding and thus prevent verdoheme formation.

Our current results have shown that, by simply replacing the *b*-type heme in Cu_BMb(*b*) with an *o*-type heme mimic, the additional hydroxyl group significantly slowed verdoheme formation (from 0.028 s⁻¹ to 0.0015 s⁻¹). Computer modeling showed that the distance between the hydroxyl of the heme *o* mimic and the distal atom of the bound oxygen is around 5.3 Å (data not shown), making it possible to form a hydrogen-bonding network by internal bridging water molecules. In the present study, a two-isomer mixture of heme *o* mimic (Figure 2, parts D and E) was used, and yet they behave like a single species in their reaction with O₂. Even though the two isomers have different orientations inside the protein, the distances between the hydroxyl group and the heme iron are the same. Therefore it might be possible for the hydroxyl group in both orientations to form a similar hydrogen-bonding network with bound O₂ through intervening water molecules that can accommodate the difference in the orientations and thus display similar reactivity. Further study using a single isomer may provide deeper insight into this proposal. Nevertheless, our results strongly support the proposal that proton delivery is essential in HCO activity. Further, the hydroxyl group in the hydroxyethylfarnesyl chain of *o*- and *a*-type hemes is instrumental in creating and maintaining the hydrogen-bonding network for proton delivery.

To provide further insight into the different reactivity of the heme types used in this study, the effect of change in redox potential due to introduction of the hydroxyl group on the heme degradation rate was also investigated. In Cu_BMb(*o*), the electron-withdrawing vinyl group in heme *b* was substituted by a more electron-donating hydroxyl ethyl group, resulting in a more electron-rich heme center in Cu_BMb(*o*) than that in Cu_BMb(*b*). Indeed, the redox potential of heme *o* in Cu_BMb(*o*) (62 mV vs NHE) was found to be 20 mV lower than that of Cu_B-

Mb(*b*) (80 mV vs NHE). The redox potential of mesoheme-incorporated Cu_BMb(*m*) is even lower (53 mV vs NHE) due to replacement of the vinyl groups with ethyl groups. Since the heme degradation rate Cu_BMb(*m*) is similar to that of Cu_BMb(*b*) and faster than that of Cu_BMb(*o*), the reduction potentials and thus the electron-donating ability of the heme center may not correlate with the HCO reactivities. These results may also explain why heme *a*, with an electron-withdrawing formyl group (Figure 2A), can still carry out similar HCO reactions as heme *o* and provide another support for the presence of the hydroxyl group, the main common functional group between the heme *a/o* and *b*, as critical for HCO activities.

Conclusions

In summary, we have replaced heme *b* with a heme *o* mimic in an engineered heme-copper site model in myoglobin. It can serve as a small stable model protein free of other chromophores for heme-copper oxidase with an *o*-type heme in the heme-copper center. The heme replacement resulted in an ~4 nm blue shift in the Soret band and ~20 mV decrease in the heme reduction potential. No correlation was found between the reduction potential or electron-donating ability and heme reactivity. Instead, kinetic studies indicate that the hydroxyl group of the hydroxyethylfarnesyl side chain of heme *o* plays a critical role in preventing the undesirable heme degradation reaction, probably through formation of a hydrogen-bonding network that facilitates proton delivery to the heme-copper center.

Acknowledgment. This material is based upon work supported by a Grant from the National Institutes of Health (GM62211).

Supporting Information Available: Complete citations of refs 6 and 14. This material is available free of charge via the Internet at <http://pubs.acs.org>.

JA052659G